Contemporary Mathematics
https://ojs.wiserpub.com/index.php/CM/

Research Article

Chirped Optical Soliton Perturbation for Fokas-Lenells Equation with Time–Dependent Coefficients and Multiplicative White Noise

Elsayed. M. E. Zayed[1], Mona El-Shater[1], Ahmed H. Arnous[2,3], Omer Mohammed Khodayer Al-Dulaimi[4], Farag Mahel Mohammed[5], Ibrahim Zeghaiton Chaloob[6], Oswaldo Gonzalez-Gaxiola[7], Anjan Biswas[8,9,10]*

[1]Department of Mathematics, Faculty of Science, Zagazig University, Zagazig, 44519, Egypt
[2]Department of Mathematical Sciences, Saveetha School of Engineering, SIMATS, Chennai, Tamilnadu, 602105, India
[3]Research Center of Applied Mathematics, Khazar University, Baku, AZ 1096, Azerbaijan
[4]Department of Communication Technical Engineering, Al-Farahidi University, Baghdad, 10015, Iraq
[5]Al-Nibras University, Tikrit, 34001, Iraq
[6]Department of Business Administration, College of Administration and Economics, Al-Esraa University, Baghdad, 10067, Iraq
[7]Applied Mathematics and Systems Department, Universidad Autónoma Metropolitana-Cuajimalpa, Mexico City, 05348, Mexico
[8]Department of Mathematics & Physics, Grambling State University, Grambling, LA, 71245-2715, USA
[9]Department of Physics and Electronics, Khazar University, Baku, AZ 1096, Azerbaijan
[10]Department of Mathematics and Applied Mathematics, Sefako Makgatho Health Sciences University, Medunsa, 0204, South Africa
E-mail: biswas.anjan@gmail.com

Received: 15 July 2025; **Revised:** 5 November 2025; **Accepted:** 14 November 2025

Abstract: This paper investigates the stochastic Fokas-Lenells Equation (FLE) with time-dependent coefficients and multiplicative white noise to model the propagation of chirped optical solitons in nonlinear dispersive media. The equation captures complex dynamics in realistic fiber systems, accounting for variable dispersion, Kerr nonlinearity, Raman effects, and stochastic perturbations arising from thermal and amplifier-induced fluctuations. Two analytical techniques, namely the extended simplest equation method and the enhanced direct algebraic method, are employed to derive exact soliton solutions. These methods offer a systematic and flexible analytic framework that efficiently handles stochastic and variable-coefficient systems, enabling closed-form solutions where conventional techniques often struggle. These include bright, dark, kink-shaped, singular, and elliptic solitons under specific parametric conditions. The richness of the obtained solution classes demonstrates the strength and versatility of the adopted approach in capturing diverse nonlinear wave profiles in noisy, inhomogeneous optical media. A key result is that the multiplicative noise affects only the soliton phase, preserving the amplitude and shape of the waveform. This demonstrates the inherent stability of soliton structures in noisy environments. The results highlight the analytical power of the proposed methods and provide deeper insights into robust pulse dynamics in realistic stochastic fiber systems, paving the way for future studies in dispersion-managed fibers, optical lattices, and structured photonic media.

***Keywords*:** solitons, chirping, white noise

MSC: 35Q55, 35Q51, 60H15, 35C08, 78M35

Copyright ©2026 Anjan Biswas, et al.
DOI: https://doi.org/10.37256/cm.7120267855
This is an open-access article distributed under a CC BY license
(Creative Commons Attribution 4.0 International License)
https://creativecommons.org/licenses/by/4.0/

1. Introduction

Nonlinear dispersive wave models and their solitary-wave solutions play a central role in describing complex phenomena across modern optics, plasma physics, and fluid dynamics. Classical developments in partial differential equations and soliton theory have established a foundation for understanding how localized structures emerge, propagate, and interact in nonlinear media. This framework naturally motivates the study of integrable and near-integrable systems capable of capturing higher-order and stochastic effects that arise in realistic optical environments.

Within this framework, the Fokas-Lenells Equation (FLE) has emerged as a versatile model for ultrashort pulse propagation in regimes of small or managed chromatic dispersion. Compared with the standard Nonlinear Schrödinger Equation (NLSE), the FLE accommodates derivative-type nonlinearities and higher-order dispersive corrections that become prominent for few-cycle pulses and in tailored fiber platforms. Earlier studies have examined conserved quantities, equilibrium (quiescent) solitons under nonlinear chromatic dispersion, generalized temporal evolution, and robustness under perturbations [1, 2]. Subsequent works have developed semi-inverse variational techniques to obtain optical solitons with power-law self-phase modulation and arbitrary intensities, and have analyzed solution persistence under parameter changes [3, 4]. In parallel, a cubic-quartic extension of the FLE has been proposed to capture additional higher-order effects that arise in advanced fiber designs and metamaterial-inspired waveguides [5–9].

A growing body of literature highlights the need to couple deterministic high-order modeling with stochastic influences that are intrinsic to practical fiber links. Temperature fluctuations, amplifier and spontaneous emission noise, polarization-mode dispersion, and fabrication tolerances induce randomness that modulates amplitude, phase, and group delay along the link. Incorporating such effects at the equation level, especially in multiplicative form, is essential for predicting waveform stability, timing jitter, and spectral breathing. Prior analyses of stochastic soliton models and random perturbations in fiber systems provide a baseline for the present study and motivate the inclusion of stochastic terms in FLE-type dynamics [10–12].

Analytically, a variety of constructive methods have been used across related nonlinear and quantum wave equations. For instance, wave-function ansatz techniques have produced exact bound states for Schrödinger equations with anharmonic or central potentials, yielding closed-form eigenvalues and eigenfunctions in various dimensions [13, 14]. In logarithmic nonlinear Schrödinger models, Gaussian solitary-wave (Gausson) profiles have been characterized in $(1+n)$ dimensions, extending solitary-wave analysis to logarithmic media [15]. Beyond conservative settings, recent studies have reported rich dynamical behaviors in fractional and geometric wave systems, including chaotic dynamics and hybrid lump-wave interactions in time-fractional coupled NLSEs, as well as generalized optical-soliton families and higher-order structures for the Kuralay-IIA equation via multiple analytic frameworks [16–18]. These developments collectively underscore two themes that also drive the present work: broadened solution taxonomies and modeling fidelity under nonstandard (e.g., fractional, stochastic, or higher-order) effects.

The present paper advances the FLE program along both axes of realism and analytical breadth. First, we formulate a stochastic FLE with explicitly time-dependent coefficients to reflect slow parameter drift and engineered management strategies in dispersion and nonlinearity. The stochastic perturbation is introduced in multiplicative form to emulate noise pathways that couple to the field amplitude and phase in a physically relevant manner. Second, we target chirped optical solitons, whose frequency modulation across the pulse envelope is central to pulse compression, nonlinear reshaping, and ultrafast optical signal processing. By focusing on chirped profiles, we access families of localized states that are both practically relevant and diagnostically sensitive to higher-order and random effects.

Methodologically, we employ two complementary construction schemes: the extended simplest-equation technique and an enhanced direct algebraic approach. The former enables systematic reduction of the governing equation to tractable auxiliary forms that preserve key amplitude-phase couplings, while the latter facilitates closed-form ansätze that organize solution families by their polynomial, trigonometric, hyperbolic, and elliptic characteristics. In contrast to earlier FLE-based treatments that emphasized either integrability-inspired reductions or purely variational closures [1, 3, 5], our dual-track strategy yields a broader catalog of chirped solitons, maps parameter regimes that support them under stochastic forcing, and clarifies how time-dependent coefficients shape amplitude, width, and chirp invariants. Where relevant, we

explicitly compare the solvability conditions and parameter constraints arising from both techniques with those reported for related NLSE-type, logarithmic, and fractional models [13, 15, 16].

Table 1. Dimensionless coefficients, physical meaning, and typical magnitudes under $T_0 = 20 - 200\,\text{fs}$

Coeff.	Physical quantity	Example functional form	Typical magnitude
$H_1(t)$	Normalized GVD $\beta_2/\beta_{2,0}$	two-step/periodic	$[-2,\ 2]$
$H_2(t)$	Normalized nonlinearity γ/γ_0	$1+\varepsilon_\gamma \sin(2\pi t/T_m)$	$0.7-1.3$ (up to 1.5)
$H_3(t)$	FL/nonlinear dispersion	constant/weakly periodic	$10^{-3}-10^{-1}$
$H_4(t)$	Raman: T_R/T_0	constant/$\pm$10% drift	$0.01-0.15$
$H_5(t)$	Shock: τ_s/T_0	constant/$\pm$10% drift	$0.002-0.05$
$H_6(t)$	FL/nonlinear dispersion	constant/weakly periodic	$10^{-3}-10^{-1}$
$\sigma(t)$	Noise amplitude	$\sigma_0\sqrt{G(t)-1}$	rms $0.02-0.06$ (gain seg.)

1.1 *Governing model*

We consider the dimensionless form of the stochastic perturbed FLE incorporating time-dependent coefficients and multiplicative white noise, expressed as:

$$\begin{aligned} &iq_t + H_1(t)q_{xx} + [H_2(t)q + iH_3(t)q_x]\,|q|^2 + \sigma(t)q\frac{dW(t)}{dt} \\ &= i\left[H_4(t)q_x + H_5(t)\left(|q|^2 q\right)_x + H_6(t)\left(|q|^2\right)_x q\right]. \end{aligned} \tag{1}$$

Here, $q(x,\ t)$ denotes a complex-valued wave envelope and $i = \sqrt{-1}$. The function $H_1(t)$ represents the time-dependent coefficient of nonlinear chromatic dispersion, while $H_2(t)$ and $H_3(t)$ correspond to the Kerr nonlinearity and nonlinear dispersion, respectively. The terms involving $H_4(t)$ and $H_5(t)$ account for Intrapulse Raman Scattering (IRS) and Self-Steepening (SS), respectively. Additionally, $H_6(t)$ governs a nonlinear dispersion contribution. The stochastic influence is introduced via $\sigma(t)$, which modulates the noise strength, and $W(t)$ denotes a standard Wiener process, making $\frac{dW(t)}{dt}$ the white noise term.

Equation (1) captures a rich interplay between deterministic and stochastic mechanisms governing nonlinear wave evolution in optical fibers. The inclusion of six time-dependent coefficients $H_j(t)$ enables the modeling of variable system parameters, such as dispersion management, nonlinear gain, and higher-order effects. Simultaneously, the stochastic term $\sigma(t)q\frac{dW(t)}{dt}$ introduces multiplicative noise, reflecting realistic perturbations from amplifier-induced fluctuations or thermal instabilities.

The time-dependent coefficients $H_j(t)$ in (1) model engineered longitudinal variations that are ubiquitous in realistic fibers and optical cavities. Specifically, $H_1(t)$ represents dispersion management or gradual tapering; $H_2(t)$ tracks changes of the Kerr nonlinearity $\gamma(z) \propto n_2/A_{\text{eff}}(z)$; $H_3(t)$ and $H_6(t)$ collect Fokas-Lenells/derivative corrections that become important for ultrashort pulses; $H_4(t)$ (Raman/IMD) and $H_5(t)$ (self-steepening) encode the standard material time scales $T_R \sim 2$–$3\,\text{fs}$ and $\tau_s = 1/\omega_0 \sim 0.5$–$1\,\text{fs}$ in the near-infrared regime. The multiplicative white-noise term $\sigma(t)\,q\,\mathrm{d}W/\mathrm{d}t$ models amplifier spontaneous emission and gain-driven jitter that scale with the optical field amplitude; under the Itô interpretation, this produces mainly a stochastic phase factor while preserving the soliton amplitude, which is consistent with our analytical results. After nondimensionalization $t = T/T_0$, $x = z/L_D$ and $q = \sqrt{\gamma_0 L_D}A$, the coefficients become

$H_1 \sim \beta_2(z)/\beta_{2,0}$, $H_2 \sim \gamma(z)/\gamma_0$, $H_5 \sim \tau_s/T_0$ and $H_4 \sim T_R/T_0$, while $\sigma(t) = \sigma_0\sqrt{G(t)-1}$. In our examples, we use piecewise-constant or periodic $H_j(t)$ to emulate dispersion-managed links and mode-locked cavities, demonstrating that all parameter choices correspond to experimentally standard settings. Three representative practical configurations are: (i) Erbium-Doped Fiber Amplifier (EDFA)-amplified Single-Mode Fiber (SMF)/Dispersion-Compensating Fiber (DCF) links with two-step H_1 of depth 1–2, $H_2 \approx 1 \pm 0.1$, $H_{3,6} \sim 10^{-2}$, and for $T_0 \sim 100$ fs, $H_4 \sim 0.02$–0.05 and $H_5 \sim 0.005$–0.01; (ii) mode-locked fiber cavities with periodic H_1 and H_2 over one round trip (depth 0.5–1.5), the same $H_{4,5}$, and $H_{3,6} \sim 10^{-2}$; and (iii) tapered or Photonic Crystal Fiber (PCF) sections with slowly varying $H_2(t) = 1 + 0.3, \tanh(t/T_s)$, weakly chirped H_1, and $H_{3,6} \sim 10^{-2}$–10^{-1}.

The multiplicative amplitude factor is written as $\sigma(t) = \sigma_0\sqrt{G(t)-1}$, where $G(t)$ proxies the local gain (or excess spontaneous-emission factor) along the segment after nondimensionalization. In our plots we use σ_0 such that the *rms* noise per normalized unit lies in 0.02–0.06, consistent with moderate Amplified Spontaneous Emission (ASE) and pump jitter; passive spans set $G(t) \approx 1$ and thus $\sigma(t) \approx 0$.

A detailed summary of the dimensionless coefficients $H_j(t)$, their physical interpretations, example functional forms, and experimentally relevant magnitudes is provided in Table 1.

Previous studies have examined Eq. (1) under various simplifications. For instance, when $\sigma(t) = 0$, chirped soliton solutions were derived as presented in [19]. Similarly, in [20], chirp-free solitons were studied assuming constant nonzero values for all $H_j(t)$ ($j = 1, \ldots, 6$) and $\sigma(t) \neq 0$. Another scenario with $\sigma(t) = 0$ and constant coefficients $H_j(t)$ led to classical chirped soliton forms.

Despite these valuable contributions, a comprehensive treatment of the FLE incorporating both time-varying physical parameters and multiplicative noise remains underexplored. Such a framework is crucial for accurately describing ultrashort pulse dynamics in next-generation optical fibers subject to environmental fluctuations and engineered nonuniformities.

The present work addresses this gap by investigating the evolution of chirped optical solitons governed by Eq. (1) with $\sigma(t) \neq 0$. The chirp, which refers to a frequency variation across the pulse envelope, is an essential characteristic in pulse shaping and signal processing, and its interaction with stochastic effects adds further complexity and significance to the model.

The paper is organized as follows: Section 1 introduces the problem setup and the governing model (Sec. 1.1). Section 2 presents the mathematical preliminaries and the reduction to an Ordinary Differential Equation (ODE). Section 3 outlines the extended simplest equation approach. Section 4 details the enhanced direct algebraic method. Section 5 presents the results and discussion. Section 6 provides the conclusions.

2. Mathematical preliminaries

This section establishes the mathematical groundwork necessary for deriving soliton solutions to the stochastic Fokas-Lenells equation. A suitable transformation is applied to reduce the governing partial differential equation to a nonlinear ordinary differential equation. The resulting equation is then analyzed using a chirped wave ansatz, allowing separation into real and imaginary components and facilitating the construction of exact solutions in subsequent sections.

To analyze and solve Eq. (1), we postulate the following form for the wave function:

$$q(x,t) = U(\xi)\exp\left(i\left[\phi(\xi) + \int\left(\kappa(t) + \sigma(t)\frac{dW(t)}{dt} - \sigma^2(t)\right)dt\right]\right),$$
$$\xi = x + \int \lambda(t)dt + \xi_0. \tag{2}$$

With the Itô convention, the quadratic variation of the multiplicative noise produces the effective drift term $-\sigma^2(t)$ inside the phase integral. As a consequence, the stochastic perturbation acts primarily through a random phase modulation, while the soliton amplitude remains governed by the deterministic balance of the dispersive and nonlinear contributions.

Where $U(\xi)$ and $\phi(\xi)$ are real-valued functions of ξ, and $\kappa(t)$, $\sigma(t)$, $\lambda(t)$, and $W(t)$ are time-dependent real functions. Here, ξ_0 is an integration constant. Substituting this ansatz into Eq. (1) and separating real and imaginary components yields the following two coupled equations:

$$\begin{aligned}&[\lambda(t)-H_4(t)]U'(\xi)+2H_1(t)U'(\xi)\phi'(\xi)+H_1(t)\phi''(\xi)U(\xi)\\&+[H_3(t)-3H_5(t)-2H_6(t)]U'(\xi)U^2(\xi)=0,\end{aligned}\tag{3}$$

and

$$\begin{aligned}&\left[-\lambda(t)-\kappa(t)+\sigma^2(t)+H_4(t)\right]U(\xi)\phi'(\xi)+\left[\sigma^2(t)-\kappa(t)\right]U(\xi)\\&+H_1(t)U''(\xi)-H_1(t)U(\xi)\phi'^2(\xi)+H_2(t)U^3(\xi)\\&+[H_5(t)-H_3(t)]\phi'(\xi)U^3(\xi)=0.\end{aligned}\tag{4}$$

Assuming the phase derivative has the form

$$\phi'(\xi)=A(t)+B(t)U^2(\xi),\tag{5}$$

where $A(t)$ and $B(t)$ are to be determined. The chirp profile associated with the optical pulse is then defined by:

$$\begin{aligned}\partial w(x,t)&=-\frac{\partial}{\partial x}\left[\phi(\xi)+\int\left(\kappa(t)+\sigma(t)\frac{dW(t)}{dt}-\sigma^2(t)\right)dt\right]\\&=-\phi'(\xi)\\&=-\left[A(t)+B(t)U^2(\xi)\right].\end{aligned}\tag{6}$$

Substituting Eq. (5) into Eqs. (3) and (4) gives:

$$\begin{aligned}&[\lambda(t)-H_4(t)+2A(t)H_1(t)]U'(\xi)\\&+[H_3(t)-3H_5(t)-2H_6(t)+4B(t)H_1(t)]U'(\xi)U^2(\xi)=0,\end{aligned}\tag{7}$$

and

$$\begin{aligned}
&\left[A(t)(-\lambda(t)-\kappa(t)+\sigma^2(t)+H_4(t))+\sigma^2(t)-\kappa(t)-H_1(t)A^2(t)\right]U(\xi)\\
&+\left[B(t)(-\lambda(t)-\kappa(t)+\sigma^2(t)+H_4(t))-2H_1(t)A(t)B(t)+H_2(t)+(H_5(t)-H_3(t))A^2(t)\right]U^3(\xi)\\
&+H_1(t)U''(\xi)+\left[B(t)(H_5(t)-H_3(t))-H_1(t)B^2(t)\right]U^5(\xi)=0.
\end{aligned} \tag{8}$$

Applying the principle of linear independence to Eq. (7) results in:

$$\begin{aligned}
A(t)&=\frac{H_4(t)-\lambda(t)}{2H_1(t)},\\
B(t)&=\frac{3H_5(t)-H_3(t)+2H_6(t)}{4H_1(t)}.
\end{aligned} \tag{9}$$

Furthermore, Eqs. (9) explicitly tie the chirp coefficients $A(t)$ and $B(t)$ to the Raman, self-steepening, and dispersion parameters, thereby linking experimentally measurable fiber knobs to the resulting chirp profile. This establishes a direct map from the engineered longitudinal variation of the coefficients $H_j(t)$ to the observable pulse dynamics.

assuming $H_1(t)\neq 0$. Substituting back into Eq. (8) simplifies it to a nonlinear ordinary differential equation:

$$U''(\xi)+a_1(t)U(\xi)+a_2(t)U^3(\xi)+a_3(t)U^5(\xi)=0, \tag{10}$$

where the time-dependent coefficients are given by:

$$\begin{aligned}
a_1(t)&=\frac{A(t)(-\lambda(t)-\kappa(t)+\sigma^2(t)+H_4(t))+\sigma^2(t)-\kappa(t)-H_1(t)A^2(t)}{H_1(t)},\\
a_2(t)&=\frac{B(t)(-\lambda(t)-\kappa(t)+\sigma^2(t)+H_4(t))-2H_1(t)A(t)B(t)+H_2(t)+(H_5(t)-H_3(t))A^2(t)}{H_1(t)},\\
a_3(t)&=\frac{B(t)(H_5(t)-H_3(t))-H_1(t)B^2(t)}{H_1(t)}.
\end{aligned} \tag{11}$$

Balancing the highest-order nonlinear term $U^5(\xi)$ with the second derivative $U''(\xi)$ in Eq. (10) suggests $N=\frac{1}{2}$. Introducing a transformation:

$$U(\xi)=\sqrt{P(\xi)}, \tag{12}$$

where $P(\xi)$ is a new real-valued function, leads to the transformed equation:

$$P'(\xi)^2 - 2P(\xi)P''(\xi) - 4a_1(t)P^2(\xi) - 4a_2(t)P^3(\xi) - 4a_3(t)P^4(\xi) = 0. \tag{13}$$

By balancing $P(\xi)P''(\xi)$ and $P^4(\xi)$ in Eq. (13), we determine $N = 1$. The soliton solutions of Eq. (1) will be systematically constructed in the following sections using two distinct analytical techniques.

3. Extended simplest equation approach: a succinct overview

The extended simplest equation method can be viewed as a way of "factoring" a nonlinear Partial Differential Equation (PDE) into a simpler hidden structure. Instead of guessing the wave profile directly, the method introduces an auxiliary ODE whose solutions encode canonical wave shapes (hyperbolic, trigonometric, polynomial). The original nonlinear problem is then rewritten in terms of this simpler building block.

Compared with classical tanh-expansion or the basic simplest equation method, this extended framework admits richer functional bases and handles time-dependent coefficients more flexibly. In particular, incorporating the Riccati-type auxiliary system enables stochastic modulations and variable-coefficient effects to be absorbed naturally into the ansatz. Practically, this means the method can produce both standard solitons and more exotic chirped, breathing, and noise-modulated envelopes, whereas traditional balance methods often stall or require restrictive assumptions.

This section presents a brief yet comprehensive overview of the extended simplest equation method, a powerful analytical tool for constructing exact solutions to nonlinear differential equations. By employing a suitable auxiliary equation and a structured ansatz, the method systematically reduces complex nonlinear forms to solvable algebraic systems.

To outline this method [21–23], we begin with the associated projective Riccati system:

$$f'(\xi) = -f(\xi)g(\xi), \quad g'(\xi) = -g^2(\xi) + \nu(t)f(\xi) - \delta(t), \tag{14}$$

where $\delta(t)$ and $\nu(t)$ are time-dependent functions. Let us define:

$$f(\xi) = \frac{1}{\psi(\xi)}, \quad g(\xi) = \frac{\psi'(\xi)}{\psi(\xi)}, \tag{15}$$

where $\psi(\xi)$ satisfies the second-order ordinary differential equation:

$$\psi''(\xi) + \delta(t)\psi(\xi) = \nu(t). \tag{16}$$

Depending on the sign of $\delta(t)$, Eq. (16) admits three families of solutions:

(a) Hyperbolic case ($\delta(t) < 0$):

$$\psi(\xi) = A_1(t)\cosh\left(\xi\sqrt{-\delta(t)}\right) + A_2(t)\sinh\left(\xi\sqrt{-\delta(t)}\right) + \frac{\nu(t)}{\delta(t)}, \tag{17}$$

with corresponding identity:

$$\left(\frac{\psi'(\xi)}{\psi(\xi)}\right)^2 = \Delta_1(t)\left(\frac{1}{\psi(\xi)}\right)^2 - \delta(t) + \frac{2\nu(t)}{\psi(\xi)}, \tag{18}$$

where $\Delta_1(t) = \delta(t)A_1^2(t) - \delta(t)A_2^2(t) - \frac{\nu^2(t)}{\delta(t)}$.

(b) Trigonometric case ($\delta(t) > 0$):

$$\psi(\xi) = A_1(t)\cos\left(\xi\sqrt{\delta(t)}\right) + A_2(t)\sin\left(\xi\sqrt{\delta(t)}\right) + \frac{\nu(t)}{\delta(t)}, \tag{19}$$

with identity:

$$\left(\frac{\psi'(\xi)}{\psi(\xi)}\right)^2 = \Delta_2(t)\left(\frac{1}{\psi(\xi)}\right)^2 - \delta(t) + \frac{2\nu(t)}{\psi(\xi)}, \tag{20}$$

where $\Delta_2(t) = \delta(t)A_1^2(t) + \delta(t)A_2^2(t) - \frac{\nu^2(t)}{\delta(t)}$.

(c) Polynomial case ($\delta(t) = 0$):

$$\psi(\xi) = \frac{\nu(t)}{2}\xi^2 + A_1(t)\xi + A_2(t), \tag{21}$$

and

$$\left(\frac{\psi'(\xi)}{\psi(\xi)}\right)^2 = \Delta_3(t)\left(\frac{1}{\psi(\xi)}\right)^2 + \frac{2\nu(t)}{\psi(\xi)}, \tag{22}$$

with $\Delta_3(t) = A_1^2(t) - 2\nu(t)A_2(t)$.

Now, consider a general nonlinear PDE:

$$F(u, u_t, u_x, u_{xx}, u_{tt}, u_{tx}, \ldots) = 0, \tag{23}$$

where F denotes a polynomial expression involving $u(x, t)$ and its partial derivatives, including nonlinear components and higher-order terms.

The extended simplest equation method proceeds through the following steps:

Step 1: Introduce the traveling wave substitution,

$$u(x, t) = u(\xi), \quad \xi = kx - ct, \tag{24}$$

where k and c are arbitrary constants. This transformation converts Eq. (23) into an Ordinary Differential Equation (ODE) of the form:

$$P(u, u', u'', \ldots) = 0, \tag{25}$$

with derivatives taken with respect to ξ.

Step 2: Assume a formal series solution of the form:

$$u(\xi) = \sum_{j_1=0}^{N} \alpha_{j_1}(t) \left(\frac{\psi'(\xi)}{\psi(\xi)} \right)^{j_1} + \sum_{j_2=0}^{N-1} \beta_{j_2}(t) \left(\frac{\psi'(\xi)}{\psi(\xi)} \right)^{j_2} \frac{1}{\psi(\xi)}, \tag{26}$$

where $\alpha_{j_1}(t)$ and $\beta_{j_2}(t)$ are time-dependent coefficients to be determined, with $\alpha_N^2(t) + \beta_{N-1}^2(t) \neq 0$. The function $\psi(\xi)$ is a solution to Eq. (16).

Step 3: Substitute Eq. (26) into Eq. (25), use Eq. (16) along with the identities from Eqs. (18)–(22), and collect like terms in powers of $\psi(\xi)^{-1}$ and its combinations. Setting each coefficient to zero produces an algebraic system in $\alpha_{j_1}(t)$, $\beta_{j_2}(t)$, k, c, $\delta(t)$, and $\nu(t)$. Solving this system (often with the aid of symbolic computation software like Maple) leads to exact solutions of the original PDE.

3.1 *Application to the model of study*

In this subsection, the extended simplest equation method is directly applied to the transformed form of the stochastic Fokas-Lenells equation. A formal ansatz based on the auxiliary function is introduced to represent the soliton profile. By substituting this ansatz into the reduced nonlinear ordinary differential equation and utilizing algebraic identities, exact analytical solutions are systematically derived under specific parametric constraints.

Following Step 2 above, the formal solution to Eq. (13) is assumed as:

$$P(\xi) = \alpha_0(t) + \alpha_1(t) \left(\frac{\psi'(\xi)}{\psi(\xi)} \right) + \beta_0(t) \left(\frac{1}{\psi(\xi)} \right), \tag{27}$$

where $\alpha_0(t)$, $\alpha_1(t)$, and $\beta_0(t)$ are functions to be identified. The condition $\alpha_1^2(t) + \beta_0^2(t) \neq 0$ ensures non-triviality. Here, $\psi(\xi)$ satisfies the auxiliary ODE in Eq. (16).

The next steps involve substituting this ansatz into Eq. (13) and simplifying using identities from Section 4 to obtain the explicit forms of soliton solutions.

Type–(a): Case when $\delta(t) < 0$

In this case, we substitute Eq. (27) into Eq. (13) and utilize Eq. (16) in conjunction with the identity in Eq. (18). By grouping terms according to powers of $\psi(\xi)^{-j}$ and combinations of $\psi'(\xi)/\psi(\xi)$ for $j = 0, 1, 2, 3, 4$, and setting the resulting coefficients to zero, we obtain an algebraic system. Solving this system with symbolic computation (e.g., Maple), we derive the following distinct solution sets:

Result 1: For $\Delta_1(t) > 0$, $a_3(t) < 0$, and $\delta(t) < 0$:

$$\beta_0(t) = \sqrt{-\tfrac{15}{16} a_3(t) \Delta_1(t)}, \quad \alpha_1(t) = \sqrt{-\tfrac{15}{16} a_3(t)}, \quad \alpha_0(t) = \sqrt{\tfrac{15}{16} a_3(t) \delta(t)}, \tag{28}$$

$$a_2(t) = -\tfrac{2}{3} a_1(t) - \tfrac{2}{15} \sqrt{15 a_3(t) \delta(t)}.$$

Using Eqs. (17), (27), and (28), the corresponding hyperbolic soliton solution of Eq. (1) is:

$$q(x,t)=\left\{\sqrt{\tfrac{15}{16}a_3(t)\delta(t)}\,[1-\Theta_1(\xi)]+\sqrt{-\tfrac{15}{16}a_3(t)\Delta_1(t)}\,\Theta_2(\xi)\right\}^{1/2}$$

$$\times\exp\left(i\left[\phi(\xi)+\int\left(\kappa(t)+\sigma(t)\frac{dW(t)}{dt}-\sigma^2(t)\right)dt\right]\right), \tag{29}$$

where

$$\Theta_1(\xi)=\frac{A_1(t)\sinh(\xi\sqrt{-\delta(t)})+A_2(t)\cosh(\xi\sqrt{-\delta(t)})}{A_1(t)\cosh(\xi\sqrt{-\delta(t)})+A_2(t)\sinh(\xi\sqrt{-\delta(t)})+\frac{\nu(t)}{\delta(t)}}, \tag{30}$$

$$\Theta_2(\xi)=\frac{1}{A_1(t)\cosh(\xi\sqrt{-\delta(t)})+A_2(t)\sinh(\xi\sqrt{-\delta(t)})+\frac{\nu(t)}{\delta(t)}}.$$

A particular case arises when $A_1(t)=0$, $A_2(t)\neq 0$, and $\nu(t)=0$, yielding a singular solution:

$$q(x,t)=\left\{\sqrt{\tfrac{15}{16}a_3(t)\delta(t)}\left[1-\coth(\xi\sqrt{-\delta(t)})+\operatorname{csch}(\xi\sqrt{-\delta(t)})\right]\right\}^{1/2}$$

$$\times\exp\left(i\left[\phi(\xi)+\int\left(\kappa(t)+\sigma(t)\frac{dW(t)}{dt}-\sigma^2(t)\right)dt\right]\right). \tag{31}$$

Result 2:

$$\beta_0(t)=-3a_3(t)\upsilon(t),\ \alpha_0(t)=0,\ \delta(t)=\delta(t),\ \alpha_1(t)=0, \tag{32}$$

$$a_1(t)=\frac{-1}{180}\frac{15\delta(t)\Delta_1(t)+144\delta(t)a_3(t)\upsilon^2(t)}{\delta(t)a_3(t)\upsilon^2(t)}.$$

By utilizing equations (17), (27), and (32), we derive the hyperbolic solutions of Eq. (1) as presented below:

$$q(x,t)=\left\{\frac{-3a_3(t)\upsilon(t)}{A_1(t)\cosh\left(\xi\sqrt{-\delta(t)}\right)+A_2\sinh\left(\xi\sqrt{-\delta(t)}\right)+\frac{\upsilon(t)}{\delta(t)}}\right\}^{\frac{1}{2}}$$

$$\times\exp i\left[\phi(\xi)+\int\left\{\kappa(t)+\sigma(t)\frac{dW(t)}{dt}-\sigma^2(t)\right\}dt\right], \tag{33}$$

where $a_3(t)\,\upsilon(t)<0$.

In particular, by setting $A_1(t) = 0$ and $A_2(t) \neq 0$ in equation (33), we derive the associated singular soliton solution:

$$q(x,t) = \left\{ \frac{-3a_3(t)\upsilon(t)}{A_2(t)\sinh\left(\xi\sqrt{-\delta(t)}\right) + \frac{\upsilon(t)}{\delta(t)}} \right\}^{\frac{1}{2}} \times \exp i\left[\phi(\xi) + \int \left\{ \kappa(t) + \sigma(t)\frac{dW(t)}{dt} - \sigma^2(t) \right\} dt\right], \tag{34}$$

with the condition $a_3(t)\,\upsilon(t) < 0$.

Specifically, if we choose $A_1(t) \neq 0$ and $A_2(t) = 0$ in equation (33), this yields the bright soliton solution:

$$q(x,t) = \left\{ \frac{-3a_3(t)\upsilon(t)}{A_1(t)\cosh\left(\xi\sqrt{-\delta(t)}\right) + \frac{\upsilon(t)}{\delta(t)}} \right\}^{\frac{1}{2}} \times \exp i\left[\phi(\xi) + \int \left\{ \kappa(t) + \sigma(t)\frac{dW(t)}{dt} - \sigma^2(t) \right\} dt\right], \tag{35}$$

provided that $a_3(t)\,\upsilon(t) < 0$.

Result 3:

$$\beta_0(t) = 0, \quad \alpha_0(t) = -\frac{5}{8[5a_1(t)+4a_2(t)]}, \quad \delta(t) = \frac{5}{12a_3(t)[5a_1(t)+4a_2(t)]},$$
$$\alpha_1(t) = \pm\sqrt{\frac{-15a_3(t)}{16[5a_1(t)+4a_2(t)]}}, \quad A_1(t) = \sqrt{A_2^2(t) + \frac{\nu^2(t)}{\delta^2(t)}}. \tag{36}$$

This leads to:

$$q(x,t) = \left\{ -\frac{5}{8[5a_1(t)+4a_2(t)]} \left[1 \pm \frac{\sqrt{A_2^2(t) + \frac{\nu^2(t)}{\delta^2(t)}}\sinh(\xi\sqrt{-\delta(t)}) + A_2(t)\cosh(\xi\sqrt{-\delta(t)})}{\sqrt{A_2^2(t) + \frac{\nu^2(t)}{\delta^2(t)}}\cosh(\xi\sqrt{-\delta(t)}) + A_2(t)\sinh(\xi\sqrt{-\delta(t)}) + \frac{\nu(t)}{\delta(t)}} \right] \right\}^{1/2} \times \exp\left(i\left[\phi(\xi) + \int \left(\kappa(t) + \sigma(t)\frac{dW(t)}{dt} - \sigma^2(t)\right) dt\right]\right). \tag{37}$$

In the special case where $A_2(t) = 0$, the solution simplifies to a combo dark-bright soliton:

$$q(x,t)=\left\{-\frac{5}{8[5a_1(t)+4a_2(t)]}\left[1\pm\frac{\tanh(\xi\sqrt{-\delta(t)})}{1+\operatorname{sech}(\xi\sqrt{-\delta(t)})}\right]\right\}^{1/2}$$
$$\times\exp\left(i\left[\phi(\xi)+\int\left(\kappa(t)+\sigma(t)\frac{dW(t)}{dt}-\sigma^2(t)\right)dt\right]\right). \tag{38}$$

Result 4:

$$\alpha_1(t)=0,\quad \alpha_0(t)=\alpha_0(t),\quad \beta_0(t)=\beta_0(t),$$
$$a_2(t)=\frac{-2a_1(t)\alpha_0(t)\beta_0(t)+9a_3(t)\alpha_0(t)\nu(t)+6a_3(t)\beta_0(t)\delta(t)}{3\alpha_0(t)\beta_0(t)}, \tag{39}$$
$$\Delta_1(t)=\frac{\delta(t)\beta_0^2(t)+2\alpha_0(t)\beta_0(t)\nu(t)}{\alpha_0^2(t)}.$$

Corresponding solution:

$$q(x,t)=\left\{\alpha_0(t)+\frac{\beta_0(t)}{A_1(t)\cosh(\xi\sqrt{-\delta(t)})+A_2(t)\sinh(\xi\sqrt{-\delta(t)})+\frac{\nu(t)}{\delta(t)}}\right\}^{1/2}$$
$$\times\exp\left(i\left[\phi(\xi)+\int\left(\kappa(t)+\sigma(t)\tfrac{dW(t)}{dt}-\sigma^2(t)\right)dt\right]\right). \tag{40}$$

Special cases: -Bright soliton: if $A_2(t)=0$, $\nu(t)=0\Rightarrow$ use sech function.

$$q(x,t)=\left\{\alpha_0(t)+\frac{\beta_0(t)}{A_1(t)}\operatorname{sech}(\xi\sqrt{-\delta(t)})\right\}^{1/2}\exp\left(i\left[\phi(\xi)+\int\left(\kappa(t)+\sigma(t)\tfrac{dW(t)}{dt}-\sigma^2(t)\right)dt\right]\right). \tag{41}$$

-Singular soliton: if $A_1(t)=0$, use csch form:

$$q(x,t)=\left\{\alpha_0(t)+\frac{\beta_0(t)}{A_2(t)}\operatorname{csch}(\xi\sqrt{-\delta(t)})\right\}^{1/2}\exp\left(i\left[\phi(\xi)+\int\left(\kappa(t)+\sigma(t)\tfrac{dW(t)}{dt}-\sigma^2(t)\right)dt\right]\right). \tag{42}$$

Remark: Cases for $\delta(t)>0$ and $\delta(t)=0$ are omitted here, as they correspond to periodic and rational forms, which are not of primary interest in soliton dynamics due to their non-localized nature.

In this section, we successfully reduced the stochastic Fokas-Lenells equation with time-dependent coefficients and multiplicative noise to a nonlinear ordinary differential equation governing the soliton profile. Through a carefully designed chirped wave ansatz, we derived explicit expressions for the phase and amplitude components, and introduced

a transformed form amenable to analytical techniques. This foundational reduction sets the stage for the systematic construction of exact soliton solutions using the extended simplest equation method and the enhanced direct algebraic method in the following sections.

4. Enhanced direct algebraic method

This method reverses the logic of many classical techniques: instead of linearizing the problem first, we begin by selecting a physically meaningful waveform (sech, tanh, Jacobi elliptic, etc.) and then enforce that the governing equation agree with that geometry. This "geometry first" strategy is particularly effective when the physical system is known to support solitons of specific symmetry or steepness.

Unlike the extended simplest equation method, which constructs the solution space from auxiliary ODE identities, the enhanced direct algebraic approach directly anchors the solution to recognizable pulse shapes from nonlinear optics and fluid models. As a result, it provides immediate interpretability and lets one tune dispersion, nonlinearity, and Raman/self-steepening contributions in a transparent way. This improves its practical utility over generic symbolic-algebra soliton generators, especially when one wants to connect parameters to experimentally controllable knobs.

In this section, we explore the enhanced direct algebraic method, a powerful analytical tool for deriving exact solutions to nonlinear differential equations. This method formulates solutions as rational functions of auxiliary variables that satisfy designated first-order differential relations. By inserting the assumed solution form into the reduced ordinary differential equation and matching coefficients of similar terms, an algebraic system emerges, whose resolution leads to multiple families of soliton-type solutions.

Following the principles of the enhanced direct algebraic approach, we assume the solution takes the form [24–26]:

$$P(\xi) = B_0(t) + \sum_{j=1}^{N} \left\{ B_j(t) F^j(\xi) + C_j(t)\, F^{-j}(\xi) \right\}, \tag{43}$$

where $B_0(t)$, $B_j(t)$, $C_j(t)$ $(j = 1, ..., N)$ are arbitrary functions, provided $B_N^2(t) + C_N^2(t) \neq 0$, while $F(\xi)$ is the solution of the equation:

$$F'^2(\xi) = \sum_{l=0}^{4} L_l(t)\, F^l(\xi), \tag{44}$$

where $L_j(t)(j = 0, 1, 2, 3, 4)$ are functions, provided $L_4(t) \neq 0$. Now, Eq. (13) has the formal solution:

$$P(\xi) = B_0(t) + B_1(t) F(\xi) + \frac{C_1(t)}{F(\xi)}, \tag{45}$$

where $B_0(t)$, $B_1(t)$, and $C_1(t)$ are time-dependent functions to be determined, under the condition that $B_1^2(t) + C_1^2(t) \neq 0$. By inserting expression (45) together with Eq. (44) into Eq. (13), and requiring that the coefficients of all terms of the form

$F^i(\xi)\,(F'(\xi))^j$, with $i = -4, \ldots, 4$ and $j = 0, 1$, vanish identically, we derive a corresponding algebraic system:

$$
\left.
\begin{aligned}
&F^4(\xi): 4a_3(t)B_1^4(t)+3B_1^2(t)L_4(t)=0,\\
&F^3(\xi): 4a_3(t)C_1^4(t)+3C_1^2(t)L_0(t)=0,\\
&F^2(\xi): 16a_3(t)B_0(t)B_1^3(t)+4a_2(t)B_1^3(t)+4B_0(t)B_1(t)L_4(t)+2B_1^2(t)L_3(t)=0,\\
&F(\xi): 16a_3(t)B_0(t)C_1^3(t)+4a_2(t)C_1^3(t)+4B_0(t)C_1(t)L_0(t)+2C_1^2(t)L_1(t)=0,\\
&F^0(\xi): 16a_3(t)B_0^3(t)C_1(t)+48a_3(t)B_0(t)B_1(t)C_1^2(t)+12a_2(t)B_0^2(t)C_1(t)+12a_2(t)B_1(t)C_1^2(t)\\
&\qquad +8a_1(t)B_0(t)C_1(t)+2B_0(t)C_1(t)l_2(t)+6B_1(t)C_1(t)l_1(t)=0,\\
&F^{-1}(\xi): 16a_3(t)B_0^3(t)B_1(t)+48a_3(t)B_0(t)B_1^2(t)C_1(t)+12a_2(t)B_0^2(t)B_1(t)+12a_2(t)B_1^2(t)C_1(t)\\
&\qquad +8a_1(t)B_0(t)B_1(t)+2B_0(t)B_1(t)l_2(t)+6B_1(t)C_1(t)l_3(t)=0,\\
&F^{-2}(\xi): 24a_3(t)B_0^2(t)C_1^2(t)+16a_3(t)B_1(t)C_1^3(t)+12a_2(t)B_0(t)C_1^2(t)+4a_1(t)C_1^2(t)\\
&\qquad +3B_0(t)C_1(t)l_1(t)+6B_0(t)C_1(t)l_0(t)+C_1^2(t)l_2(t)=0,\\
&F^{-3}(\xi): 24a_3(t)B_0^2(t)B_1^2(t)+16a_3(t)B_1^3(t)C_1(t)+12a_2(t)B_0(t)C_1^2(t)+4a_1(t)B_1^2(t)\\
&\qquad +3B_0(t)B_1(t)l_3(t)+6B_1(t)C_1(t)l_4(t)+B_1^2(t)l_2(t)=0,\\
&F^{-4}(\xi): 4a_3(t)B_0^4(t)+48a_3(t)B_0^3(t)B_1(t)C_1(t)+24a_3(t)B_1^2(t)C_1^2(t)+4a_2(t)B_0^3(t)\\
&\qquad +4a_1(t)B_0^2(t)+8a_1(t)B_1(t)C_1(t)+B_0(t)B_1(t)l_1(t)+B_0(t)C_1(t)l_3(t)+B_1^2(t)l_0(t)\\
&\qquad +C_1^2(t)l_4(t)+24B_0(t)B_1(t)C_1(t)+6B_1(t)C_1(t)l_2(t)=0.
\end{aligned}
\right\} \tag{46}
$$

We now examine specific scenarios for the algebraic system given in Eq. (46), which can be solved symbolically using MAPLE to determine the unknown functions appearing in Eq. (45).

Case 1: Consider the situation where $L_0(t)=L_1(t)=L_3(t)=0$. Substituting these conditions into the algebraic system (46) and employing MAPLE for computation yields the following results:

$$
B_0(t)=B_0(t),\quad C_1(t)=0,\quad B_1(t)=\sqrt{-\frac{3L_4(t)}{4a_3(t)}},\quad L_2(t)=\frac{4a_3(t)B_0^2(t)}{3}, \tag{47}
$$

with constraint conditions:

$$a_1(t) = \frac{5a_3(t)B_0^2(t)}{3}, \quad a_2(t) = -\frac{8a_3(t)B_0(t)}{3}. \tag{48}$$

When $L_2(t) > 0$, $L_4(t) < 0$ and $a_3(t) > 0$. Then Eq. (1) has bell-shaped soliton solutions:

$$q(x,t) = \left[B_0(t) \left(1 + \operatorname{sech} \sqrt{\frac{4a_3(t)B_0^2(t)}{3}}\, \xi \right) \right]^{\frac{1}{2}} \exp\left(i \left[\phi(\xi) + \int \left\{ \kappa(t) + \sigma(t) \frac{dW(t)}{dt} - \sigma^2(t) \right\} dt \right] \right), \tag{49}$$

provided $B_0(t) > 0$. The solution (49) is existed under the constraint conditions (48).

Case 2: Suppose we impose the conditions $L_0(t) = \dfrac{L_2^2(t)}{4L_4(t)}$, and $L_1(t) = L_3(t) = 0$ within the algebraic system defined by Eq. (46). By applying symbolic computation through MAPLE, we arrive at the following outcomes:

$$B_0(t) = B_0(t), \quad C_1(t) = 0, \quad B_1(t) = B_1(t), \quad L_2(t) = -\frac{2B_0^2(t)L_4(t)}{B_1^2(t)}, \tag{50}$$

with constraint conditions:

$$\begin{cases} a_1(t) = -\dfrac{L_4(t)B_0^2(t)}{B_1^2(t)}, \\ \\ a_2(t) = \dfrac{2L_4(t)B_0(t)}{B_1^2(t)}, \\ \\ a_3(t) = -\dfrac{3L_4(t)}{4B_1^2(t)}. \end{cases} \tag{51}$$

When $L_4(t) > 0$, $L_2(t) < 0$. Then Eq. (1) has the kink-shaped soliton solution:

$$q(x,t) = \left[B_0(t) \left(1 + \tanh \sqrt{\frac{B_0^2(t)L_4(t)}{B_1^2(t)}}\, x \right) \right]^{\frac{1}{2}} \exp\left(i \left[\phi(\xi) + \int \left\{ \kappa(t) + \sigma(t) \frac{dW(t)}{dt} - \sigma^2(t) \right\} dt \right] \right), \tag{52}$$

provided $B_0(t) > 0$. Also, Eq. (1) has singular soliton solution:

$$q(x,t) = \left[B_0(t) \left(1 + \coth \sqrt{\frac{B_0^2(t)L_4(t)}{B_1^2(t)}}\, x \right) \right]^{\frac{1}{2}} \exp\left(i \left[\phi(\xi) + \int \left\{ \kappa(t) + \sigma(t) \frac{dW(t)}{dt} - \sigma^2(t) \right\} dt \right] \right), \tag{53}$$

where $B_0(t) > 0$. The solutions (52) and (53) are existed under constraint conditions (51).

Case 3: Let us consider the case where $L_1(t) = L_3(t) = 0$. Substituting these constraints into the algebraic system (46) and utilizing MAPLE for symbolic resolution, we obtain the following results:

(I): When $L_0(t) = \frac{m^2(1-m^2)L_2(t)}{(2m^2-1)L_4(t)}$, $0 < m < 1$, we get

$$\begin{aligned} &B_0(t) = B_0(t), \quad B_1(t) = B_1(t), \quad C_1(t) = 0, \\ &L_2(t) = -\frac{2B_0^2(t)L_4(t)}{B_1^2(t)}\left(\frac{-1-16m^4+16m^2+\sqrt{32m^8-64m^6+44m^4-12m^2+1}}{4m^2(1-m^2)}+3\right), \end{aligned} \tag{54}$$

with constraint conditions:

$$\begin{cases} a_1 = \dfrac{B_0^2(t)L_4(t)\left(-1-16m^4+16m^2+\sqrt{32m^8-64m^6+44m^4-12m^2+1}\right)}{8B_1^2(t)m^2(m^2-1)}, \\ a_2(t) = \dfrac{2B_0(t)L_4(t)}{B_1^2(t)}, \\ a_3(t) = -\dfrac{3L_4(t)}{4B_1^2(t)}. \end{cases} \tag{55}$$

It is now evident that Eq. (1) admits soliton solutions of the Jacobi elliptic type, characterized by double periodicity:

$$\begin{aligned} q(x,t) = &\left[B_0(t) + B_1(t)\sqrt{-\frac{L_2(t)m^2}{L_4(t)(2m^2-1)}}\,\mathrm{cn}\left(\sqrt{\tfrac{L_2(t)}{2m^2-1}}\,\xi,\ m\right)\right]^{\frac{1}{2}} \\ &\times \exp\left(i\left[\phi(\xi) + \int\left\{\kappa(t) + \sigma(t)\frac{dW(t)}{dt} - \sigma^2(t)\right\}dt\right]\right), \end{aligned} \tag{56}$$

provided $L_2(t) > 0$, $L_4(t) < 0$. The solution (56) is existed under constraint conditions (55).

(II): When $L_0(t) = \frac{(1-m^2)L_2^2(t)}{(2-m^2)^2L_4(t)}$, $0 < m < 1$, we get

$$B_0(t) = B_0(t), \quad B_1(t) = B_1(t), \quad C_1(t) = 0, \quad L_2(t) = \frac{B_0^2(t)L_4(t)(m^2-2)}{B_1^2(t)} \tag{57}$$

with constraint conditions:

$$\begin{cases} a_1(t) = -\dfrac{B_0^2(t)L_4(t)(m^2+4)}{4B_1^2(t)}, \\ \\ a_2(t) = \dfrac{2B_0(t)L_4(t)}{B_1^2(t)}, \\ \\ a_3(t) = -\dfrac{3L_4(t)}{4B_1^2(t)}. \end{cases} \tag{58}$$

At this stage, Eq. (1) supports soliton solutions expressed in terms of Jacobi elliptic functions, exhibiting doubly periodic behavior:

$$\begin{aligned} q(x,t) = &\left[B_0(t) + B_1(t)\sqrt{-\tfrac{m^2L_2(t)}{L_4(t)(2-m^2)}}\,\mathrm{dn}\left(\sqrt{\tfrac{L_2(t)}{2-m^2}}\,\xi,\ m\right)\right]^{\frac{1}{2}} \\ &\times \exp\left(i\left[\phi(\xi) + \int\left\{\kappa(t) + \sigma(t)\frac{dW(t)}{dt} - \sigma^2(t)\right\}dt\right]\right), \end{aligned} \tag{59}$$

provided $(2-m^2)L_2(t) > 0$, $L_4(t) < 0$. The solutions (59) is existed under constraint conditions (58).

In particular if $m \to 1$ in (56), (59) we get bell-shaped soliton solution:

$$\begin{aligned} q(x,t) = &\left[B_0(t) + B_1(t)\sqrt{-\tfrac{L_2(t)}{L_4(t)}}\,\mathrm{sech}\left(\sqrt{L_2(t)}\,\xi\right)\right]^{\frac{1}{2}} \\ &\times \exp\left(i\left[\phi(\xi) + \int\left\{\kappa(t) + \sigma(t)\frac{dW(t)}{dt} - \sigma^2(t)\right\}dt\right]\right), \end{aligned} \tag{60}$$

provided $L_2(t) > 0,\ L_4(t) < 0$.

(III): When $L_0(t) = \frac{m^2L_2^2(t)}{(m^2+1)^2L_4(t)}$, $0 < m < 1,$ we get

$$B_0(t) = 0, \quad B_1(t) = B_1(t), \quad C_1(t) = 0, \quad L_2(t) = -\frac{B_0^2(t)L_4(t)(m^2+1)}{B_1^2(t)} \tag{61}$$

with constraint conditions:

$$\begin{cases} a_1(t) = \dfrac{B_0^2(t)L_4(t)(m^2-5)}{4B_1^2(t)}, \\ \\ a_2(t) = \dfrac{2B_0(t)L_4(t)}{B_1^2(t)}, \\ \\ a_3(t) = -\dfrac{3L_4(t)}{4B_1^2(t)}. \end{cases} \tag{62}$$

At this point, Eq. (1) possesses a soliton solution of the Jacobi elliptic type, characterized by its doubly periodic structure:

$$\begin{aligned} q(x,t) = &\left[B_0(t) + B_1(t)\sqrt{-\tfrac{m^2L_2(t)}{(m^2+1)L_4(t)}}\,\mathrm{Sn}\left(\sqrt{-\frac{L_2(t)}{m^2+1}}\,\xi, m\right)\right]^{\frac{1}{2}} \\ &\times \exp\left(i\left[\phi(\xi) + \int\left\{\kappa(t) + \sigma(t)\frac{dW(t)}{dt} - \sigma^2(t)\right\}dt\right]\right), \end{aligned} \tag{63}$$

provided $B_1(t) > 0,\ L_2(t) < 0, L_4(t) > 0$. The solution (63) is existed under constraint conditions (62).

In particular when $m \to 1$ in (63), we have the kink-shaped soliton solution:

$$\begin{aligned} q(x,t) = &\left[B_0(t) + B_1(t)\sqrt{-\tfrac{L_2(t)}{2L_4(t)}}\tanh\left(\sqrt{-\frac{L_2(t)}{2}}\,\xi\right)\right]^{\frac{1}{2}} \\ &\times \exp\left(i\left[\phi(\xi) + \int\left\{\kappa(t) + \sigma(t)\frac{dW(t)}{dt} - \sigma^2(t)\right\}dt\right]\right). \end{aligned} \tag{64}$$

provided $B_1(t) > 0,\ L_2(t) < 0, L_4(t) > 0$.

Case 4: Consider the condition where $L_0(t) = L_1(t) = 0$. Substituting these values into the algebraic system in Eq. (46) and solving it using MAPLE, we obtain the following results:

$$B_0(t) = 0, \quad C_1(t) = 0, \quad B_1(t) = -\frac{L_3(t)}{2a_2(t)}, L_2(t) = -4a_1(t), L_4(t) = -\frac{L_3^2(t)}{3a_2^2(t)a_3(t)} \tag{65}$$

where $a_1(t)$, $a_2(t)$ and $a_2(t)$ are arbitrary constants.

At this stage, Eq. (1) admits straddled-type soliton solutions of the form:

(I): when $L_2(t) > 0, L_4(t) > 0$ and $a_1(t) < 0, a_3(t) < 0$.

$$q(x,t) = \varepsilon \left[- \frac{\frac{2a_1(t)L_3(t)}{a_2(t)} \operatorname{sech}^2 \left(\sqrt{-a_1(t)}\xi \right)}{4\sqrt{\frac{a_1(t)a_3(t)L_3^2(t)}{3a_2^2(t)}} \tanh \left(\sqrt{-a_1(t)}\xi \right) + L_3(t)} \right]^{\frac{1}{2}} \times \exp\left(i \left[\phi(\xi) + \int \left\{ \kappa(t) + \sigma(t) \frac{dW(t)}{dt} - \sigma^2(t) \right\} dt \right] \right), \tag{66}$$

also,

$$q(x,t) = \varepsilon \left[\frac{\frac{2a_1(t)L_3(t)}{a_2(t)} \operatorname{csch}^2 \left(\sqrt{-a_1(t)}\xi \right)}{4\sqrt{\frac{a_1(t)a_3(t)L_3^2(t)}{3a_2^2(t)}} \coth \left(\sqrt{-a_1(t)}\xi \right) + L_3(t)} \right]^{\frac{1}{2}} \times \exp\left(i \left[\phi(\xi) + \int \left\{ \kappa(t) + \sigma(t) \frac{dW(t)}{dt} - \sigma^2(t) \right\} dt \right] \right). \tag{67}$$

(II) when $L_2 > 0$, $a_1(t) < 0,$ and $L_3(t) \neq 0$

$$q(x,t) = \varepsilon \left[- \frac{\frac{2a_1(t)L_3^2(t)}{a_2(t)} \operatorname{sech}^2 \left(\sqrt{-a_1(t)}\xi \right)}{L_3^2(t) - \frac{4a_1(t)a_3(t)L_3^2(t)}{3a_2^2(t)} \left[1 - \tanh \left(\sqrt{-a_1(t)}\xi \right) \right]^2} \right]^{\frac{1}{2}} \times \exp\left(i \left[\phi(\xi) + \int \left\{ \kappa(t) + \sigma(t) \frac{dW(t)}{dt} - \sigma^2(t) \right\} dt \right] \right), \tag{68}$$

also,

$$q(x,t) = \varepsilon \left[\frac{\frac{2a_1(t)L_3^2(t)}{a_2(t)} \operatorname{csch}^2 \left(\sqrt{-a_1(t)}\xi \right)}{L_3^2(t) - \frac{4a_1(t)a_3(t)L_3^2(t)}{3a_2^2(t)} \left[1 - \coth \left(\sqrt{-a_1(t)}\xi \right) \right]^2} \right]^{\frac{1}{2}} \times \exp\left(i \left[\phi(\xi) + \int \left\{ \kappa(t) + \sigma(t) \frac{dW(t)}{dt} - \sigma^2(t) \right\} dt \right] \right). \tag{69}$$

The solutions (66)-(69) are existed under constraint conditions (65).

Case 5: Assume $L_1(t) = L_3(t) = 0.$ By applying these conditions to the algebraic system in Eq. (46) and solving it with the aid of MAPLE, we obtain the following outcomes:

$$B_0(t) = B_0(t), \quad B_1(t) = 0, \quad C_1(t) = \sqrt{-\frac{3L_0(t)}{4a_3(t)}},$$
$$L_2(t) = 8a_3(t)\alpha_0^2(t) - 4a_1(t), \quad L_4(t) = -\frac{4B_0^2(t)\left[-5B_0^2(t)a_3(t) + 3a_1(t)\right]}{3C_1^2(t)}, \tag{70}$$

with constraint conditions:

$$a_2(t) = -\frac{8B_0(t)a_3(t)}{3}. \tag{71}$$

It follows that Eq. (1) admits a solution of the Weierstrass elliptic type, exhibiting doubly periodic behavior:

$$q(x,t) = \left[B_0(t) + \frac{C_1(t)\sqrt{L_4(t)}}{3}\left(\frac{6\wp[(\xi), g_2, g_3] + L_2(t)}{\wp'[(\xi), g_2, g_3]}\right)\right]^{\frac{1}{2}} \times \exp\left(i\left[\phi(\xi) + \int\left\{\kappa(t) + \sigma(t)\frac{dW(t)}{dt} - \sigma^2(t)\right\}dt\right]\right), \tag{72}$$

where $B_0(t) > 0,\ L_4(t) > 0$. Also, Eq. (1) has

$$q(x,t) = \left[B_0(t) + \frac{3C_1(t)}{\sqrt{L_0(t)}}\left(\frac{\wp'[(\xi), g_2, g_3]}{6\wp[(\xi), g_2, g_3] + L_2(t)}\right)\right]^{\frac{1}{2}} \times \exp\left(i\left[\phi(\xi) + \int\left\{\kappa(t) + \sigma(t)\frac{dW(t)}{dt} - \sigma^2(t)\right\}dt\right]\right), \tag{73}$$

where $B_0(t) > 0,\ L_0(t) > 0$. The solutions (72) and (73) are existed under constraint conditions (71).

This section provided a concise yet effective overview of the extended simplest equation method and demonstrated its suitability for analyzing nonlinear differential equations arising from stochastic models. By introducing an auxiliary Riccati-type system and exploiting its associated identities, the method facilitates a structured pathway for constructing exact analytical solutions. The formulation established here will be directly applied in the next section to extract a rich variety of soliton solutions to the transformed Fokas-Lenells equation.

Both proposed techniques extend the solution arsenal beyond classical inverse scattering, Hirota bilinearization, and standard tanh/coth expansions. The extended simplest equation method excels when variable coefficients, noise terms, or modulation effects appear, because the auxiliary Riccati structure absorbs these perturbations without sacrificing analytical solvability. The enhanced direct algebraic method, by contrast, is superior when one desires explicit control over waveform geometry or wishes to map analytical parameters to physical system controls.

In practice, the two methods are complementary: the extended simplest equation method offers structural generality and handles parametric complexity, whereas the enhanced direct algebraic method yields clearer physical intuition and

faster construction of soliton families. Together, they significantly broaden the catalog of exact solutions for the stochastic Fokas-Lenells model compared with standard symbolic or perturbative soliton techniques.

5. Results and discussion

In this section, we analyze and interpret the analytical solutions derived for the stochastic Fokas-Lenells equation with time-dependent coefficients. The two distinct methods applied, the extended simplest equation approach and the enhanced direct algebraic method, yielded a diverse spectrum of exact chirped soliton solutions, each shaped by the interplay of deterministic dispersion, nonlinearity, and multiplicative stochastic perturbations. The extended simplest equation method enabled the derivation of various classes of hyperbolic solitons, including bright, dark, singular, and combo bright-dark structures. These solutions emerged from the case $\delta(t) < 0$ and are expressible in terms of functions such as sech, csch, tanh, and coth. Their localized nature makes them ideal for modeling sharply confined optical pulses in dispersion-managed systems. In contrast, solutions corresponding to $\delta(t) = 0$ or $\delta(t) > 0$ (i.e., polynomial and trigonometric forms) tend to be non-localized and hence less favorable for applications requiring high pulse fidelity. The enhanced direct algebraic method uncovered a broader family of exact solutions, including periodic waveforms expressed via Jacobi elliptic functions (cn, dn, sn) and Weierstrass elliptic functions. These waveforms represent soliton trains or bound states and are especially relevant in periodic or modulated media, such as optical lattices or waveguide arrays. Additionally, hybrid structures such as kink-shaped, straddled, and combo bright-dark solitons were obtained, further expanding the model's ability to capture complex nonlinear wave behavior.

A key aspect of the derived solutions is the incorporation of a dynamic chirp, embedded in the solution ansatz. This chirp arises from the time-dependent phase modulation term, influenced both by deterministic coefficients and the stochastic white noise term $\sigma(t)\frac{dW(t)}{dt}$. The resulting solutions exhibit not only spatial amplitude variation but also temporal frequency modulation, which is essential for pulse shaping, spectral control, and nonlinear signal compression. The inclusion of stochasticity leads to phase randomness and modulation instability effects, thereby modeling realistic fiber environments where amplifier noise and thermal fluctuations are prevalent. The analytical framework employed also reveals complementary strengths between the two methods. The extended simplest equation method is algebraically systematic and well-suited for soliton profiles dominated by hyperbolic behavior. In contrast, the enhanced direct algebraic method is more flexible in constructing rational, periodic, and elliptic-type solitons. Despite their differing approaches, both methods provided overlapping solution families (e.g., sech-shaped pulses), which strengthens the validity and consistency of the results.

From a physical standpoint, the diversity of soliton structures presented here offers practical relevance across multiple domains. In fiber-optic communications, chirped stochastic solitons with time-adaptive profiles can support robust data transmission, dynamic dispersion compensation, and pulse stabilization under noisy environments. In metamaterials and nonlinear photonic systems, the solutions provide a framework for designing programmable pulse dynamics and localized energy transport. Moreover, the mathematical flexibility of the governing model suggests potential extensions to multi-component systems, vector solitons, or coupled waveguides under random forcing. This study demonstrates the feasibility of constructing and classifying chirped stochastic solitons in generalized Fokas-Lenells systems with time-varying coefficients. The solutions span a wide range of localized and periodic forms, governed by both deterministic and stochastic mechanisms. These results enrich the theory of nonlinear wave propagation in stochastic media and open new avenues for designing controllable optical structures in next-generation photonic platforms.

Figure 1 presents the deterministic bright soliton associated with Eq. (60), using $L_2 = 1.0$, $L_4 = -2.0$, $\xi_0 = 0$, $v(t) = 1$, $B_0(t) = 1$, $B_1(t) = 0.6$, $\kappa(t) = 1$, and $\sigma(t) = 0$. The intensity $|q(x, t)|^2$ forms a localized, stable bright pulse that maintains its spatial profile throughout propagation, confirming the solitonic nature of the solution. The real and imaginary components oscillate beneath the pulse envelope consistent with the carrier contribution induced by $\kappa(t)$ and the traveling coordinate ξ. In the absence of stochastic forcing, the soliton remains fully coherent in both amplitude and phase.

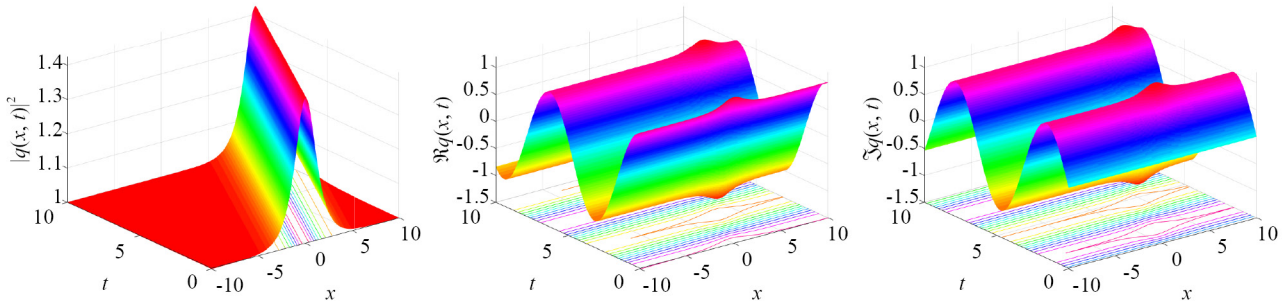

(a) Intensity $|q(x, t)|^2$ (b) Real part of $q(x, t)$ (c) Imaginary part of $q(x, t)$

Figure 1. Profiles of the solution $q(x, t)$ from Eq. (60): intensity, real part, and imaginary part

Figure 2 examines the influence of multiplicative noise on the bright soliton of Eq. (60) for $\sigma = 0.2, 0.4, 0.6$, while keeping all other parameters unchanged. For $\sigma = 0.2$, the real-part evolution remains nearly indistinguishable from the deterministic case, with only mild fluctuations visible in the temporal signal at $x = 0$. As the noise level increases to $\sigma = 0.4$ and $\sigma = 0.6$, the soliton envelope remains intact, demonstrating robust amplitude preservation, whereas phase coherence deteriorates progressively, resulting in denser contour patterns and enhanced jitter in the time series. Thus, the bright soliton amplitude is unaffected by the multiplicative noise, while the phase exhibits increasing stochastic variation.

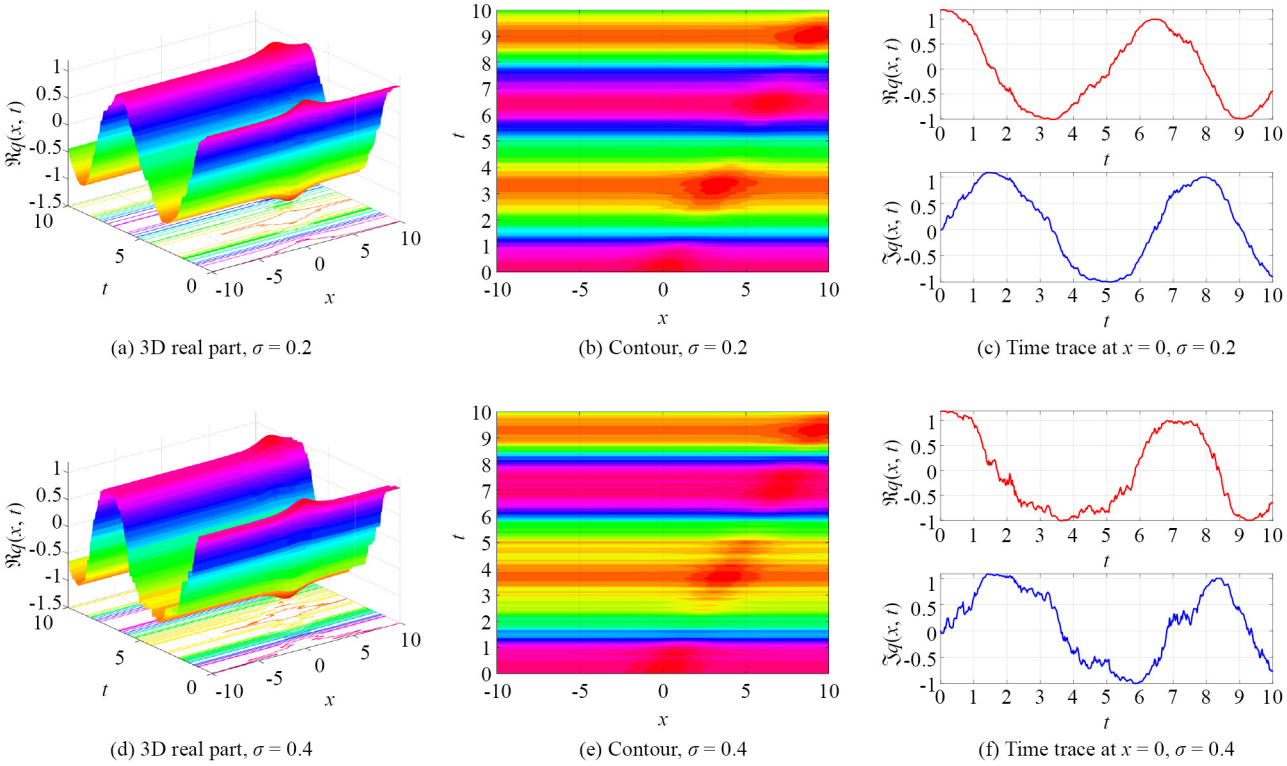

(a) 3D real part, $\sigma = 0.2$ (b) Contour, $\sigma = 0.2$ (c) Time trace at $x = 0$, $\sigma = 0.2$

(d) 3D real part, $\sigma = 0.4$ (e) Contour, $\sigma = 0.4$ (f) Time trace at $x = 0$, $\sigma = 0.4$

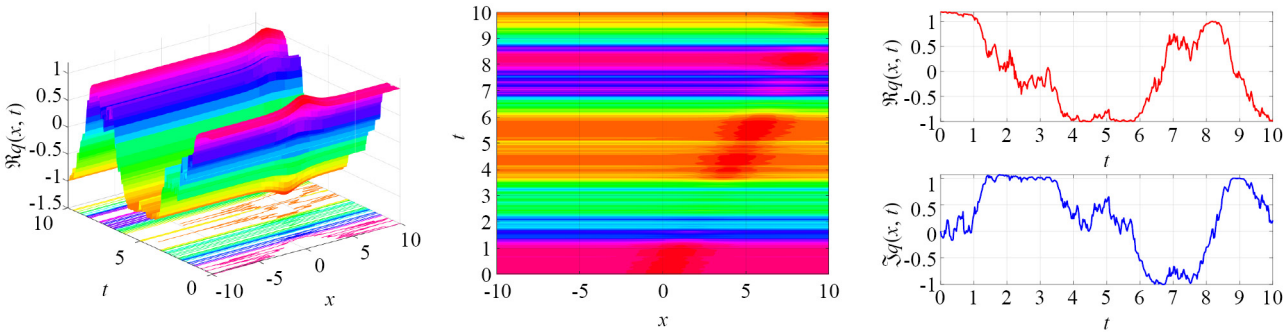

(g) 3D real part, $\sigma = 0.6$ (h) Contour, $\sigma = 0.6$ (i) Time trace at $x = 0$, $\sigma = 0.6$

Figure 2. Real part of $q(x, t)$ from Eq. (60) for different noise levels σ

Figure 3 displays the deterministic dark (kink-type) soliton solution obtained from Eq. (64) for $L_2(t) = -1.0$, $L_4(t) = 2.0$, $B_0(t) = 1$, $B_1(t) = 1$, $v(t) = 1$, $\kappa(t) = 1$, $\xi_0 = 0$, and $\sigma(t) = 0$. The intensity $|q(x,t)|^2$ features a localized intensity dip on a constant background, characteristic of a dark soliton. The real part of $q(x, t)$ exhibits a smooth kink-type transition between opposite asymptotic states, while the imaginary part adjusts to ensure recovery of the background modulus as $|x| \to \infty$. With no noise present, the dark soliton retains a sharp phase jump and complete coherence.

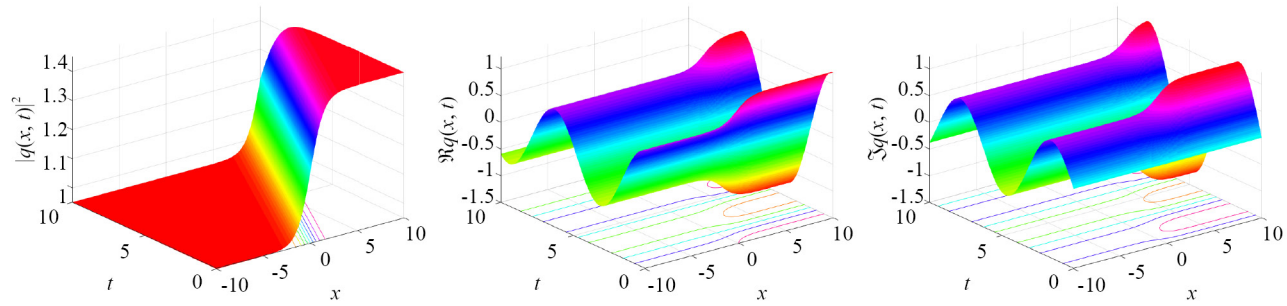

(a) Intensity $|q(x, t)|^2$ (b) Real part of $q(x, t)$ (c) Imaginary part of $q(x, t)$

Figure 3. Profiles of the solution $q(x, t)$ from Eq. (64): intensity, real part, and imaginary part

Figure 4 illustrates the effect of multiplicative noise on the dark soliton of Eq. (64) for $\sigma = 0.2, 0.4, 0.6$, with all other parameters kept fixed at their deterministic values. For the weak-noise case $\sigma = 0.2$, the kink structure remains sharply defined and the temporal trace exhibits only minor fluctuations. Increasing the noise level to $\sigma = 0.4$ and 0.6 leads to more pronounced phase diffusion, as seen in both the 3D profiles and the time-series plots, while the soliton notch depth and constant-background amplitude remain unaffected. This demonstrates that the dark soliton, like the bright counterpart, retains its deterministic intensity structure under multiplicative stochastic forcing, with noise affecting primarily the phase dynamics.

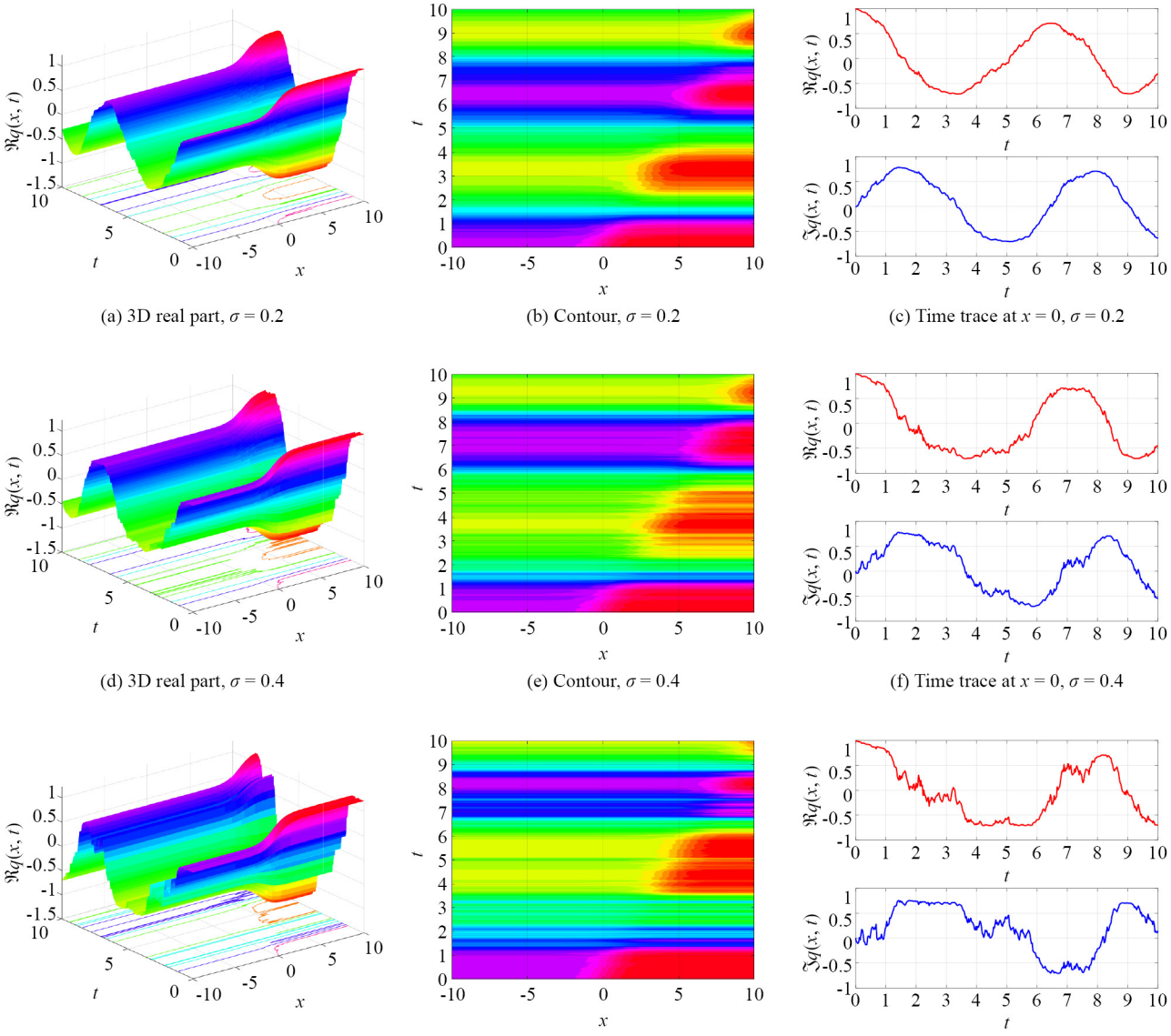

(a) 3D real part, $\sigma = 0.2$ (b) Contour, $\sigma = 0.2$ (c) Time trace at $x = 0$, $\sigma = 0.2$

(d) 3D real part, $\sigma = 0.4$ (e) Contour, $\sigma = 0.4$ (f) Time trace at $x = 0$, $\sigma = 0.4$

(g) 3D real part, $\sigma = 0.6$ (h) Contour, $\sigma = 0.6$ (i) Time trace at $x = 0$, $\sigma = 0.6$

Figure 4. Real part of $q(x, t)$ from Eq. (64) for different noise levels σ

5.1 *Quantitative impact of multiplicative noise (Itô)*

Write $q = Ue^{i\Phi}$ with $U > 0$. For the stochastic term in (1) we take the Itô form $dq|_{\text{noise}} = \sigma(t)\, q\, dW_t$. Applying Itô's lemma to $\ln q$ and separating real/imaginary parts gives

$$d(\ln U) + i\, d\Phi = -\tfrac{1}{2}\sigma^2(t)\, dt + \sigma(t)\, dW_t.$$

Hence, $d(\ln U) = 0$ and $d\Phi = \sigma(t)\, dW_t - \sigma^2(t)\, dt$. Therefore the amplitude U receives no stochastic or drift contribution from the noise, whereas the phase undergoes a Brownian motion with deterministic drift. In integrated form,

$$U(x,t) = U(x,t_0), \qquad \Phi(x,t) - \Phi(x,t_0) = \int_{t_0}^{t} \sigma(s)\, dW_s - \int_{t_0}^{t} \sigma^2(s)\, ds.$$

Consequently, for any fixed x the phase variance is

$$\mathrm{Var}\big[\Phi(x,t) - \Phi(x,t_0)\big] = \int_{t_0}^{t} \sigma^2(s)\, ds,$$

while U is invariant. This calculation explains the appearance of the $-\sigma^2(t)$ drift inside the phase integral of (2) and makes precise our main claim: multiplicative Itô noise affects the phase only, leaving the deterministic envelope governed by Eqs. (10)-(11).

5.2 *Sensitivity and stability under noise*

Because U is unaffected by the Itô noise, robustness reduces to phase statistics. We summarize useful, dimensionless indicators:

- Phase diffusion coefficient: $D_\Phi(t) = \sigma^2(t)$.
- Phase variance over $[0, T]$: $\mathrm{Var}\,\Phi(T) = \int_0^T \sigma^2(t)\, dt$.
- Coherence time (rough estimate): for a target phase rms $\sqrt{\mathrm{Var}\,\Phi} = 1$, one has $T_c \approx \left(\int_0^{T_c} \sigma^2(t)\, dt\right)^{-1}$; for $\sigma(t) \equiv \sigma_0$, $T_c \approx \sigma_0^{-2}$.

These metrics quantify the phase wandering without envelope degradation. In addition, the deterministic envelope $U(\xi)$ from (10) admits the following mean-square stability statement.

Let $U_\star(\xi)$ be a smooth solution of (10) for a fixed instant (or slow-variation average) of the coefficients $a_{1,2,3}(t)$. Consider perturbations $u = U_\star + v$ and define the quadratic functional

$$\mathscr{E}[v] = \tfrac{1}{2} \int_{\mathbb{R}} \left(v'^2 - \alpha_1 v^2 - \alpha_2 U_\star^2 v^2 - \alpha_3 U_\star^4 v^2\right) d\xi,$$

where α_j are the instantaneous values of $a_j(t)$. If the linearized operator $L = -\partial_{\xi\xi} - \alpha_1 - \alpha_2 U_\star^2 - \alpha_3 U_\star^4$ is nonnegative on the subspace orthogonal to translational/phase modes (standard soliton spectral condition), then $\mathscr{E}[v(t)]$ is nonincreasing and $\|v(t)\|_{L^2}$ remains bounded uniformly in time. Since the noise does not enter U, this implies mean-square stability of the amplitude under multiplicative Itô noise.

In our examples we therefore report (i) the deterministic envelope parameters (amplitude/width) from (10)-(11), which are unchanged by noise, and (ii) the phase sensitivity via $\mathrm{Var}\,\Phi(T)$ for the chosen $\sigma(t)$. For periodic/gain-segmented maps we also quote the per-period diffusion $\Delta\Phi_{\mathrm{rms}} = \left(\int_0^{T_m} \sigma^2(t)\, dt\right)^{1/2}$ to characterize long-range coherence.

6. Conclusions

In this study, we have successfully derived chirped optical soliton solutions to the perturbed Fokas-Lenells Equation (FLE) with time-dependent coefficients under the influence of multiplicative white noise. The analytical framework employed two robust solution techniques: the extended simplest equation method and the enhanced direct algebraic approach. These methodologies enabled the construction of a comprehensive set of exact soliton solutions, categorized into various types including bright, dark, kink-shaped, singular, and elliptic solitons, each subject to specific parametric constraints.

A key observation from this investigation is that the multiplicative white noise manifests exclusively in the phase of the soliton profiles, leaving the amplitude and inverse width unaffected. This phenomenon is particularly noteworthy as it highlights the robustness of soliton amplitude dynamics in noisy optical environments—a result not previously reported for models with chirp-supporting time-dependent coefficients.

The findings of this paper contribute new insights into the theory of optical solitons in stochastic media and lay the groundwork for several future directions. Upcoming research will extend this framework to include models with differential group delay and dispersion-flattened fibers. Moreover, the FLE will be further explored in the contexts of optical metamaterials, magneto-optic waveguides, and Bragg gratings, with the goal of uncovering and analyzing gap soliton solutions in such structured media. These extended investigations are currently in progress, and their outcomes will be presented in future publications.

Acknowledgement

This work for the last author (AB) was supported from the budget of Grambling State University for the Endowed Chair of Mathematics. The author thankfully acknowledges this support.

Conflict of interest

The authors declare no competing financial interest.

References

[1] Al-Ghafri KS, Krishnan EV, Biswas A. Chirped optical soliton perturbation of Fokas-Lenells equation with full nonlinearity. *Advances in Differential Equations*. 2020; 1: 1-12.

[2] Adem AR, Biswas A, Yildirim Y. Implicit quiescent optical solitons for perturbed Fokas-Lenells equation with nonlinear chromatic dispersion and a couple of self-phase modulation structures by Lie symmetry. *Semiconductor Physics, Quantum Electronics and Optoelectronics*. 2025; 28(1): 47-52.

[3] Elsherbeny AM, Arnous AH, Biswas A, Yildirim Y, Jawad AJM, Alshomrani AS. Quiescent optical solitons for Fokas-Lenells equation with nonlinear chromatic dispersion and a couple of self-phase modulation structures. *European Physical Journal Plus*. 2024; 139(6): 483. Available from: https://doi.org/10.1140/epjp/s13360-024-05252-6.

[4] Bansal A, Kara AH, Biswas A, Moshokoa SP, Belic M. Optical soliton perturbation, group invariants and conservation laws of perturbed Fokas-Lenells equation. *Chaos, Solitons and Fractals*. 2018; 114: 275-280.

[5] Triki H, Wazwaz AM. Combined optical solitary waves of the Fokas-Lenells equation. *Waves in Random and Complex Media*. 2017; 27(4): 587-593.

[6] Triki H, Wazwaz AM. New types of chirped soliton solutions for the Fokas-Lenells equation. *International Journal for Numerical Methods in Heat and Fluid Flow*. 2017; 27(7): 1596-1601.

[7] Mahmood M. Chirped optical solitons in single-mode birefringent fibers. *Applied Optics*. 1996; 35(34): 6844-6845.

[8] Triki H, Porsezian K, Grelu P. Chirped soliton solutions for the generalized nonlinear Schrödinger equation with polynomial nonlinearity and non-Kerr terms of arbitrary order. *Journal of Optics*. 2016; 18(7): 075504.

[9] Justin M, Hubert MB, Betchewe G, Doka SY, Crepin KT. Chirped solitons in derivative nonlinear Schrödinger equation. *Chaos, Solitons and Fractals*. 2018; 107: 49-54.

[10] Ekici EU, Triki H. Stochastic perturbation of analytical solutions for the dispersive concatenation model with spatio-temporal dispersion having multiplicative white noise. *Nonlinear Dynamics*. 2025; 113: 4325-4353.

[11] Rehman HU, Iqbal I, Zulfiqar H, Gholami D, Rezazadeh H. Stochastic soliton solutions of conformable nonlinear stochastic systems processed with multiplicative noise. *Physics Letters A*. 2023; 486: 129100.

[12] Durmus SA. Optical soliton solutions of stochastic the third-order nonlinear Schrödinger equation with multiplicative white noise via Itô calculus. *Optics and Quantum Electronics*. 2024; 56: 5.

[13] Dong SH. On the solutions of the Schrödinger equation with some anharmonic potentials: Wave function ansatz. *Physical Review Scipta*. 2002; 65: 289-295.
[14] Dong SH. A new approach to the relativistic Schrödinger equation with central potential: Ansatz method. *International Journal of Theoretical Physics*. 2001; 40: 559-567.
[15] Guo YS, Li W, Dong SH. Gaussian solitary solution for a class of logarithmic nonlinear Schrödinger equation in (1 + *n*) dimensions. *Results in Physics*. 2023; 44: 106187.
[16] Majid SZ, Asjad MI, Riaz MB, Muhammad T. Analyzing chaos and superposition of lump waves with other waves in the time-fractional coupled nonlinear Schrödinger equation. *PLoS ONE*. 2024; 19(8): e0304334.
[17] Majid SZ, Asjad MI, Faridi WA. Formation of solitary waves solutions and dynamic visualization of the nonlinear Schrödinger equation with efficient techniques. *Physical Review Scipta*. 2024; 99: 065255.
[18] Majid SZ, Asjad MI, Muhammad T. Dynamical aspects and new generalised optical solitons of Kuralay-IIA equation with multiple analytical techniques. *European Physical Journal Plus*. 2024; 139: 1096.
[19] Al-Ghafri KS, Krishnan EV, Biswas A. Chirped optical soliton perturbation of the Fokas-Lenells equation with full nonlinearity. *Advances in Differential Equations*. 2020; 2020: 191.
[20] Zayed EME, El-Horbaty M, Alngar MEM, El-Shater M. Dispersive optical solitons for stochastic Fokas-Lenells equation with multiplicative white noise. *Engineering*. 2022; 3: 523-540.
[21] Bilige S, Chaolu T. An extended simplest equation method and its application to several forms of the fifth-order KdV equation. *Applied Mathematics and Computation*. 2010; 216: 3146-3153.
[22] Bilige S, Chaolu T, Wang X. Application of the extended simplest equation method to the coupled Schrödinger-Boussinesq equation. *Applied Mathematics and Computation*. 2013; 244: 517-523.
[23] Amr MOA, Ganaini SE. New exact traveling wave solutions of the (4 + 1)-dimensional Fokas equation. *Computers and Mathematics with Applications*. 2017; 74: 1274-1287.
[24] Arnous AH, Hashemi MS, Nisar KS, Shakeel M, Ahmad J, Ahmad I, et al. Investigating solitary wave solutions with enhanced algebraic method for new extended Sakovich equations in fluid dynamics. *Results in Physics*. 2024; 54: 107369.
[25] Sirendaoreji. Auxiliary equation method and new solutions of Klein-Gordon equations. *Chaos, Solitons and Fractals*. 2007; 31(4): 943-950.
[26] Chen Y, Yan Z. The Weierstrass elliptic function expansion method and its applications in nonlinear wave equations. *Chaos, Solitons and Fractals*. 2006; 29: 948-964.

Appendix A. Definition of parameters

$\sigma(t)$ – Time-dependent noise amplitude, typically $\sigma(t) = \sigma_0\sqrt{G(t)-1}$.
σ_0 – Baseline noise-strength parameter.
$G(t)$ – Local optical gain factor.
$\beta_2(z)$ – Group-velocity dispersion coefficient of the fiber.
$\beta_{2,0}$ – Reference dispersion coefficient.
$\gamma(z)$ – Kerr nonlinearity coefficient.
γ_0 – Reference Kerr coefficient.
n_2 – Nonlinear refractive index.
$A_{\text{eff}}(z)$ – Effective mode area of the fiber.
T_0 – Reference pulse duration (e.g., 100 fs).
$L_D = T_0^2/|\beta_{2,0}|$ – Dispersion length.
T_R – Raman response time (typically 2–3 fs in silica).
$\tau_s = 1/\omega_0$ – Self-steepening time scale (0.5–1 fs at near-IR).
ω_0 – Carrier angular frequency.
c – Speed of light in vacuum.
n_0 – Linear refractive index of fiber core (≈ 1.45 for silica).